

Titanium abundances in late-type stars

I. 1D non-LTE modelling in benchmark dwarfs and giants

J. W. E. Mallinson¹, K. Lind¹, A. M. Amarsi², P. S. Barklem², J. Gruber², A. K. Belyaev³, K. Youakim¹

¹ Department of Astronomy, Stockholm University, AlbaNova University Centre, Roslagstullsbacken, SE-106 91 Stockholm, Sweden
e-mail: jack.mallinson@astro.su.se

² Theoretical Astrophysics, Department of Physics and Astronomy, Uppsala University, Box 516, SE-751 20 Uppsala, Sweden

³ Department of Theoretical Physics and Astronomy, Herzen University, St. Petersburg, Riv Moyka, 191186 Russia

ABSTRACT

Context. The titanium abundances of late-type stars are important tracers of Galactic formation history. However, abundances inferred from Ti I and Ti II lines can be in stark disagreement in very metal-poor giants. Departures from local thermodynamic equilibrium (LTE) have a large impact on the minority neutral species and thus influence the ionisation imbalance, but satisfactory non-LTE modelling for both dwarfs and giants has not been achieved in the literature.

Aims. The reliability of titanium abundances is reassessed in benchmark dwarfs and giants using a new non-LTE model 1D model atmospheres.

Methods. A comprehensive model atom was compiled with a more extended level structure and newly published data for inelastic collisions between Ti I and neutral hydrogen.

Results. In 1D LTE, the Ti I and Ti II lines agree to within 0.06 dex for the Sun, Arcturus, and the very metal-poor stars HD84937 and HD140283. For the very metal-poor giant HD122563, the Ti I lines give an abundance that is 0.47 dex lower than that from Ti II. The 1D non-LTE corrections can reach +0.4 dex for individual Ti I lines and +0.1 dex for individual Ti II lines, and they reduce the overall ionisation imbalance to -0.17 dex for HD122563. However, the corrections also increase the imbalance for the very metal-poor dwarf and sub-giant to around 0.2 dex.

Conclusions. Using 1D non-LTE reduces the ionisation imbalance in very metal-poor giants but breaks the balance of other very metal-poor stars, consistent with conclusions drawn in the literature. To make further progress, consistent 3D non-LTE models are needed.

Key words. atomic processes — radiative transfer — line: formation — Stars: abundances — Stars: late-type

1. Introduction

In the era of the European Space Agency *Gaia* mission (Gaia Collaboration et al. 2016) and large spectroscopic datasets from current and upcoming million-star surveys such as the Large Sky Area Multi-Object Fibre Spectroscopic Telescope (Zhao et al. 2012), Apache Point Observatory Galactic Evolution Experiment (Majewski et al. 2017), William Herschel Telescope Enhanced Area Velocity Explorer (Dalton et al. 2018), 4-metre Multi-Object Spectrograph Telescope (de Jong et al. 2019), and the Galactic Archaeology with High-Efficiency and high-Resolution Mercator Echelle Spectrograph (Buder et al. 2021), precision spectroscopy is becoming increasingly important for understanding the history and evolution of the Milky Way thanks to the accuracy and detail of the information being received. For example, current and future observations of stars with peculiar chemical abundance patterns, especially in the metal-poor regime, shed light on the assembly of the early Galaxy and its enrichment by supernova explosions (Nissen & Gustafsson 2018; Helmi 2020).

In this context, titanium is an element of high astrophysical interest. Ti I and Ti II lines are observed throughout a wide range of stars and produce numerous spectral lines. Thus, they are commonly used to calculate titanium abundances and fundamental stellar parameters such as effective temperature (T_{eff}) and surface gravity ($\log(g)$), and can also be a proxy for metal-

licity. Moreover, as titanium is an α -element, its abundances can trace stars of different ages (Nissen et al. 2020) due to the titanium output difference between Type Ia and core-collapse supernovae. Hence, the Galactic thin and thick discs separate out in the [Ti/Fe] versus [Fe/H] plane (Bensby et al. 2014). As such, accurate titanium abundance measurements can give insight into the formation and evolution of the Galaxy.

The success of these types of studies critically depends on the accuracy of the inferred titanium abundances. In late-type stars, it is usually possible to infer titanium abundances from both Ti I and Ti II lines. The level of ionisation balance, $\Delta_{\text{I-II}} \equiv A(\text{Ti})_{\text{Ti I}} - A(\text{Ti})_{\text{Ti II}}$, can therefore be measured, with non-zero values indicative of some deficiency in the spectral models.

One such deficiency could be the assumption of local thermodynamic equilibrium (LTE), as commonly assumed in classical spectroscopic analyses. In this approximation, the populations of excited and ionised states of titanium follow the Saha-Boltzmann distributions. In reality, similarly to neutral iron, the neutral minority species is prone to departures from LTE: the supra-thermal ultraviolet (ultraviolet) radiation field typically leads to over-ionisation (Bergemann 2011). This effect grows towards lower metallicities, where ultraviolet photons can travel through the atmosphere with even less impediment; thus, both the excess radiation and the LTE error increase.

For example, Scott et al. (2015) find $\Delta_{\text{I-II}} = -0.15$ dex for the Sun when using a 3D hydrodynamic model solar atmosphere

and 3D LTE radiative transfer. By employing non-LTE corrections computed on a (3D) model atmosphere, [Scott et al. \(2015\)](#) find a better agreement between the two species, $\Delta_{I-II} = -0.09$ dex. As the authors discuss, consistent 3D non-LTE modelling using improved data for inelastic collisions with neutral hydrogen may be needed to fully resolve these remaining ionisation imbalances.

For stars other than the Sun, all titanium abundance analyses to date have been based on 1D model atmospheres. In the absence of 3D non-LTE models, 1D non-LTE is expected to be more reliable than 1D LTE or 3D LTE, at least for neutral iron ([Amarsi et al. 2016](#); [Nordlander et al. 2017](#)). The most comprehensive 1D non-LTE models to date were recently presented by [Sitnova et al. \(2020\)](#). The authors used the 1D non-LTE code DETAIL ([Przybilla et al. 2011](#)) and employed a large model atom utilising, for the first time, ab initio inelastic hydrogen collisions. For the Sun, they find $\Delta_{I-II} = -0.07$ in 1D LTE, which is in fact similar to the 1D LTE results presented by [Scott et al. \(2015\)](#). [Sitnova et al. \(2020\)](#) find this improves to -0.03 dex in 1D non-LTE.

However, there are larger discrepancies in the metal-poor regime. For the very metal-poor giant HD122563, [Sitnova et al. \(2020\)](#) report $\Delta_{I-II} = -0.4$ in 1D LTE. This becomes less severe in 1D non-LTE, $\Delta_{I-II} = -0.2$. Unfortunately, 1D non-LTE instead worsens the ionisation imbalance for the other very metal-poor stars. In 1D LTE, they find $\Delta_{I-II} = +0.05$ and -0.03 dex for the benchmark stars HD84937 and HD140283; these change to 0.17 and 0.11 dex, respectively.

It is not clear from where exactly the large ionisation imbalances found by [Sitnova et al. \(2020\)](#) in 1D non-LTE originate. In this context, it is important to note that different groups have reported different 1D non-LTE results for other iron-peak elements. In particular, for copper, [Shi et al. \(2018\)](#) report discrepancies of 0.25 dex, 0.38 dex, and 0.69 dex for HD84937, HD140283, and HD122563, respectively, between their 1D non-LTE results and those of [Andrievsky et al. \(2018\)](#). As such, it is worthwhile to test whether the ionisation imbalances can be due to deficiencies in the non-LTE models, rather than, for example, failures of the 1D model atmospheres.

This work presents an independent 1D non-LTE study of titanium abundances in late-type benchmark stars. Compared to [Sitnova et al. \(2020\)](#), the results presented here are based on a different non-LTE code and a new model atom with higher un-collapsed energy levels utilising a more up-to-date prescription for the inelastic collisions with neutral hydrogen. This non-LTE model is used in an attempt to solve the imbalance for the Sun, dwarfs, and giants at once. The rest of this article is structured as follows. The non-LTE model is presented in Section 2, and the analysis is described in Section 3. The results for the Sun, the giant Arcturus, the very metal-poor stars HD84937 and HD140283, and the very metal-poor giant HD122563 are presented in Section 4, and the work is concluded in Section 5.

2. Method

2.1. Overview

The non-LTE calculations and theoretical stellar spectra were performed using Balder ([Amarsi et al. 2018b](#)). This code is based on Multi3D ([Leenaarts & Carlsson 2009](#)) with updates to the parallelisation scheme and background opacities ([Amarsi et al. 2018b](#)) and the statistical equilibrium solver ([Amarsi et al. 2019](#)).

Sections 2.2–2.5 describe the raw data based on which the model atom was constructed. Section 2.6 then describes the reduction process of the atom. In summary, the reduced model atom, illustrated in Fig. 1, contains the following:

587 energy levels, of which 459 are of Ti I and 127 are of Ti II, and the ground state of Ti III is included; 4 784 bound-bound radiative transitions; and 586 photo-ionisation transitions.

2.2. Energy levels

The predicted and observed energy levels of Ti I and Ti II were taken from [Kurucz \(2016\)^{1,2}](#), which was also used by [Sitnova et al. \(2020\)](#), and are included in the Vienna Atomic Line Database 3 (VALD3) ([Ryabchikova et al. 2015](#)) database. Specifically, the files called gf220X.gam and gf220X.lin were used, where X is 0 or 1. The [Kurucz \(2016\)](#) database contains nearly 18 000 bound fine-structure levels for Ti I and Ti II. These level data were combined and reduced as discussed in Section 2.6.

2.3. Radiative transitions

Data for around 6 million bound-bound transitions were extracted from [Kurucz \(2016\)](#). This dataset contains more than 5 million transitions for Ti I alone. These data were reduced as described in Section 2.6. For a subset of lines, experimentally measured *f*-values from [Wood et al. \(2013\)](#) and [Lawler et al. \(2013\)](#) were used. These are the same lines that are used for the abundance analysis in Section 3.

Photo-ionisation cross-sections for Ti I were adopted from the [Nahar \(2020\)](#) database³. Levels from [Kurucz \(2016\)](#) were cross-referenced to match the Nahar-OSU-Radiative-Atomic-Data (NORAD) database for the initial and target states of photo-ionisation transitions from [Nahar \(2020\)](#) by comparing their electron configurations and terms. Unique matches were found for all but 167 highly excited Ti I levels in the reduced model atom, none of which had an energy below 3.7eV; the majority were above 6.2eV. For these unmatched levels, the hydrogenic approximation was used ([Mihalas 1978](#)).

2.4. Inelastic hydrogen collisions

Inelastic hydrogen collision data are needed for both bound-bound and charge transfer processes. They are particularly important for metal-poor stellar atmospheres due to the lower electron densities. Therefore, changes in hydrogen collision rate coefficients may have a large impact on the spectra produced. The impact of hydrogen collision processes on the spectra and thus the abundances derived has been shown to be important for other elements ([Bergemann & Gehren 2008](#); [Lind et al. 2009](#); [Osorio et al. 2015](#); [Amarsi et al. 2018a](#); [Reggiani et al. 2019](#); [Amarsi et al. 2019](#); [Sitnova et al. 2022](#)).

Initial studies of the non-LTE effects on titanium in stellar atmospheres ([Bergemann 2011](#); [Sitnova et al. 2016](#)) were carried out using the Drawin formula ([Drawin 1968, 1969](#); [Steenbock & Holweger 1984](#); [Lambert 1993](#)), allowing a scaling factor S_H to be chosen to minimise the scatter in derived abundances across observed lines in the Sun. These works found that describing the hydrogen collisions in this manner did not work well for metal-poor stars ($[Fe/H] < -2$), giving an ionisation imbalance be-

¹ kurucz.harvard.edu/atoms/2200

² kurucz.harvard.edu/atoms/2201

³ <https://norad.astronomy.osu.edu/>

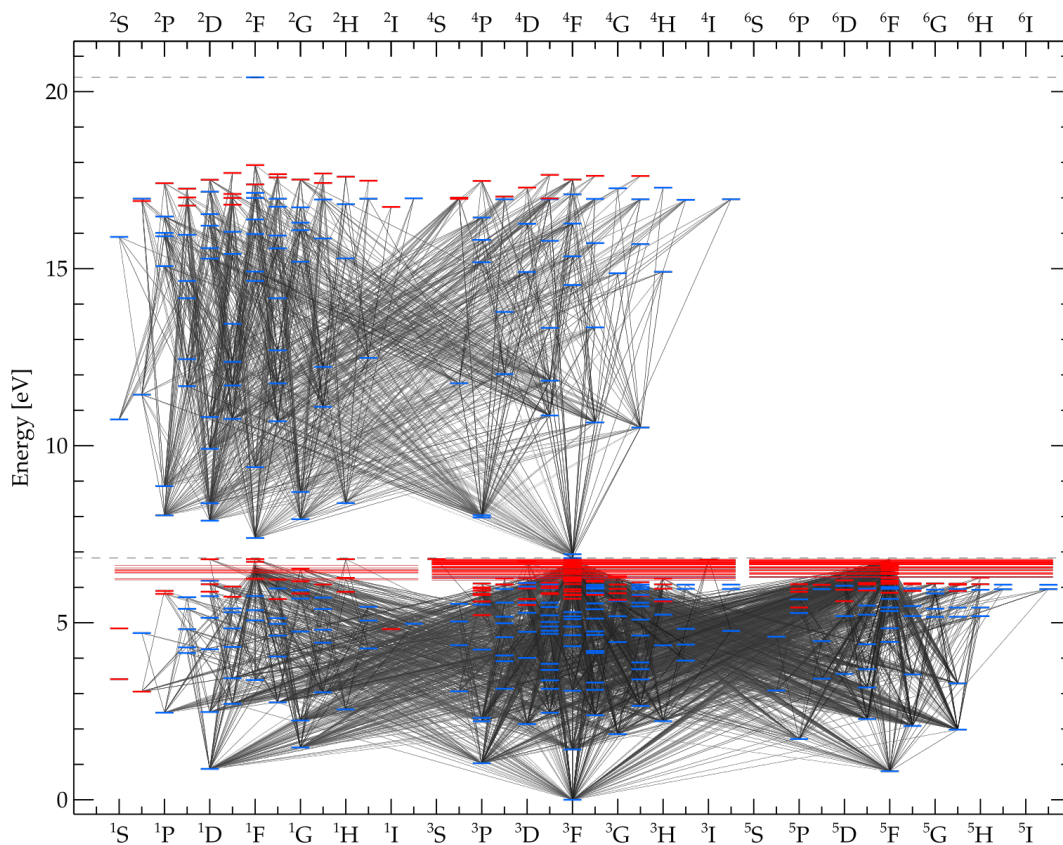


Fig. 1. Term diagram of the reduced atom showing the energies for possible bound-bound transitions of Ti I (lower half) and Ti II (upper half). Transitions are shown by black lines, with darker lines representing a higher oscillator strength. Blue marks show the observed energy levels, and red marks show levels that are theoretically predicted.

tween Ti I and Ti II that was larger than that found later using quantum mechanical calculations for hydrogen collisions (Sitnova et al. 2020). This is not unexpected, due to the large discrepancy between the Drawin formula results and those from full quantum mechanical calculations (Barklem et al. 2011).

Unfortunately, full quantum mechanical calculations of such processes are to date only available for neutral lithium (Belyaev & Barklem 2003; Barklem et al. 2003), sodium (Belyaev et al. 1999; Barklem et al. 2010; Belyaev et al. 2010), magnesium (Belyaev et al. 2012; Barklem et al. 2012; Guitou et al. 2015), and calcium (Belyaev et al. 2019). For other species, especially more complex atoms, one must resort to asymptotic model calculations based on simplified electronic structure and collision dynamics. Such approaches include the asymptotic model from Belyaev (2013), the asymptotic model from Barklem (2016), and the simplified method of Belyaev et al. (2017) and Belyaev & Voronov (2018). The asymptotic model of Barklem (2016) is based on linear combinations of atomic orbitals (LCAO) for the ionic-covalent interactions at avoided ionic crossings, which are expected to be the dominant mechanism where applicable. The others are based on a fit to calculations where the ionic-covalent interactions are taken from a semi-empirical formula (Olson et al. 1971).

Asymptotic model calculations based on LCAO were carried out by Grumer & Barklem (2020) for processes on neutral titanium, while the simplified method was applied in Sitnova et al. (2020) to both neutral and singly ionised titanium. The

bound-bound excitation rates for neutral titanium are compared in Fig. 2, and the charge transfer (ion-pair production) rates involving neutral titanium in Fig. 3. In Fig. 3 good agreement can be seen for the most important charge transfer transitions: those with large rate coefficients. However, the two datasets differ for processes with low rates, a behaviour also seen for bound-bound processes in Fig. 2. The larger scatter seen in the data from Grumer & Barklem (2020) is due to the explicit consideration of angular momentum coupling in the LCAO approach (that is, the L and S quantum numbers in LS coupling), which is not treated in the simplified approach.

In this work, the collision rate coefficients for bound-bound transitions in Ti I and its charge transfer rates to Ti II were taken from Grumer & Barklem (2020)⁴, and Ti II bound-bound rates were taken from Sitnova et al. (2020)⁵. This resulted in data for the most important transitions, but not all. For bound-bound transitions in Ti I involving states above the ionic limit, where the energy is within 0.754 eV (the electron affinity of hydrogen) of the ionised ground state, the ionic crossing mechanism does not apply, and an alternate mechanism must be at work. In these cases, the Kaulakys (1991) free electron model can be used to estimate the cross-sections and rate coefficients, via a momentum transfer mechanism. It has been argued in earlier work (Amarsi et al. 2018a) that the contribution from this mechanism should

⁴ <https://github.com/barklem/public-data>

⁵ http://www.non-lte.com/ti_h.html

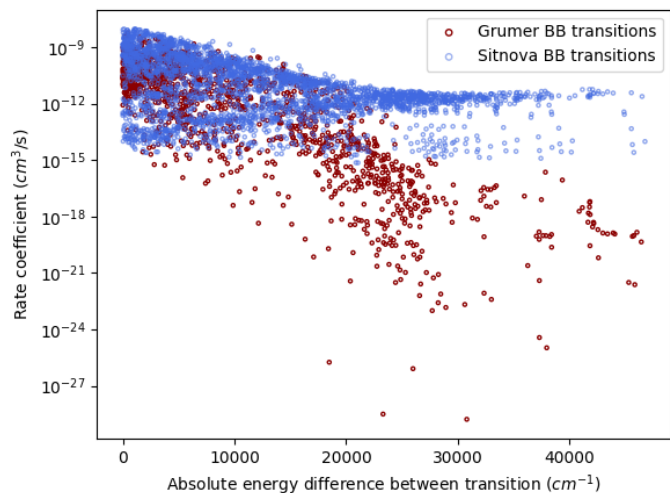


Fig. 2. Ti I bound-bound de-excitation rate coefficients as a function of the energy difference between transitions. Red points are from Grumer & Barklem (2020), and blue points are from Sitnova et al. (2020).

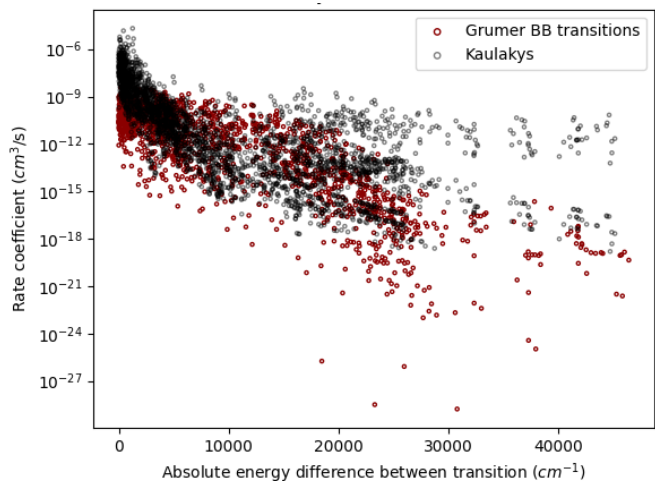


Fig. 4. Comparison between de-excitation rate coefficients from Grumer & Barklem (2020) (red points) and the rates calculated using the Kaulakys code for the same transitions (black points). The relationship found here is the same as in Amarsi et al. (2018a).

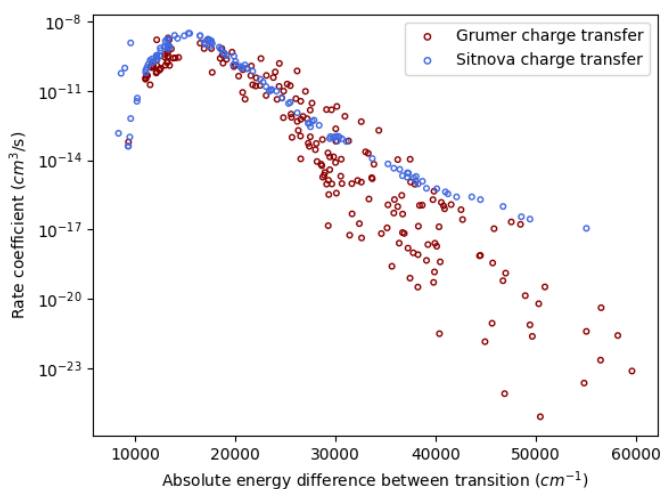


Fig. 3. Comparison of charge transfer rates for the reaction $\text{Ti I} + \text{H} \rightarrow \text{Ti II} + \text{H}^-$. Red points show data from Grumer & Barklem (2020) and blue points data from Sitnova et al. (2020), as in Fig. 2.

be added to the ionic crossing contribution, though the validity of the free electron model for low-lying states is questionable. The results of the free electron model calculations for all bound-bound transitions are shown in Fig. 4 and compared to the Grumer & Barklem (2020) results. Following Amarsi et al. (2018a), the two contributions were added together and their impact on abundance is found to be below 0.1 dex in all stars.

2.5. Electron collisions

Titanium has no advanced quantum mechanical data for electron collisions for a majority of states, and so all transitions were calculated using the semi-empirical recipes from van Regemorter (1962) for excitation and Cox (2000) for ionisation. Due to the dominance of hydrogen collisions, especially in metal-poor stars, the approximations made for electrons are found to have a small impact on the resulting abundances.

2.6. Atom reduction

The complete model atom contains thousands of levels and millions of radiative transitions, and it required reduction to make the non-LTE calculations feasible, even in 1D. To begin with, all fine structure was removed. Moreover, Ti I levels above 6.2 eV with identical parity, electron configuration, and multiplicity were merged to form super-levels and affected lines merged to form super-lines, following Lind et al. (2017). This created a smaller atom of 587 total energy levels and 50 000 transitions, which was still too large to be practical. Ti II levels within 2.7 eV of the ionisation limit were cut due to their low population in late-type stellar atmospheres.

Further reductions were made by considering the radiative brackets $|n_i R_{ij} - n_j R_{ji}|$ for different bound-bound radiative transitions. This quantity gives an estimate of the relative importance of a radiative transition to the statistical equilibrium: the lower the value, the less important it is and the safer it is to remove it. While this requires an individual depth point to be chosen, the choice does not exert much influence on the overall transition hierarchy (Lind et al. 2017). By comparing the radiative bracket of the Sun and HD 84937, 4 784 of the most important bound-bound radiative transitions were selected, and the rest were discarded, resulting in the final reduced atom.

To reduce the computational cost further, the photoionisation cross-sections were interpolated onto a common wavelength grid with fixed logarithmic steps, reducing the number of unique wavelength values from over 3 million to just over 38 000. This reduced computation time and memory requirements since, although the total number of wavelengths did not vary dramatically, it allowed Balder to treat each set of identical wavelength values as a single one during the run. While unlikely to cause a significant change, the accuracy of the interpolation was checked in two ways: first, by removing 10% of the Nahar (2015) data before interpolation, re-calculating their values, and comparing them to the original cross-sections of the removed data; secondly, by manual inspection when interpolating all wavelengths to ensure all resonances and features were still retained in the interpolated model.

The final reduced atom is illustrated in Fig. 1, which demonstrates the complexity of the atom, even after collapsing levels. It contains 459 Ti I levels under its ionisation potential of 6.828 eV,

Table 1. Stellar parameters of the studied benchmark stars.

Star	T_{eff} K	$\log(g)$ cm s ⁻²	[Fe/H]	ξ km s ⁻¹	Ref.
Sun	5772	4.44	0.00	0.9	a, d
Arcturus	4286	1.64	-0.53	1.3	b, d
HD84937	6356	4.06	-2.06	1.2	b, d
HD140283	5792	3.65	-2.36	1.3	c, d
HD122563	4636	1.40	-2.50	1.8	c, d

Notes. ^(a) Solar T_{eff} and $\log(g)$ from Prša et al. (2016). ^(b) T_{eff} and $\log(g)$ from Heiter et al. (2015). ^(c) T_{eff} and $\log(g)$ from Karovicova et al. (2020). ^(d) [Fe/H] and ξ from Lind et al. (2022).

127 Ti II levels that reach up to 2.5eV below the ionisation limit, and the Ti III ground state. This atom was run in non-LTE to produce the departure coefficients, $n_{\text{NLTE}}/n_{\text{LTE}}$, shown in Fig. 5. When generating synthetic spectra for diagnostic spectral lines, the departure coefficients were redistributed onto the complete model atom, which contains fine structure, but with the theoretical levels removed.

2.7. Atom comparison

This atom contains more unmerged levels than used previously in Sitnova et al. (2020). This was done to examine the influence these high energy levels have on titanium abundance predictions. More levels are also coupled with hydrogen collisions via the use of the Kaulakys principle for the higher energy levels above the ionic limit of Ti I. The average f -values are calculated in this paper using the experimental data of Wood et al. (2013) and Lawler et al. (2013) where possible, whereas Sitnova et al. (2020) used the database of R. Kurucz, although it was stated that the comparison was made, and the shift found to be minor, at an average of $\log(gf_{\text{lab}}) - \log(gf_{\text{Kurucz}}) = -0.05 \pm 0.28$ dex.

3. Analysis of benchmark stars

Five well-known benchmark stars were analysed using high-resolution optical spectra for the Sun, Arcturus, HD84937, HD140283, and HD122563. The same observational data used in Scott et al. (2015) were used for the Sun, and the observational data from Lind et al. (2022) were used for all other stars. The same stellar parameters were adopted as in that work, shown in Table 1. In summary, Lind et al. (2022) used interferometric T_{eff} for Arcturus, HD122563, and HD140283, while T_{eff} for HD84937 was calculated from its surface-brightness relationship (Heiter et al. 2015). Except for the Sun, $\log(g)$ was computed from mass to radius relations for all stars. [Fe/H] and microturbulence parameters were adopted from Lind et al. (2022), who determined them simultaneously by enforcing a flat trend in LTE abundance and an equivalent width of Fe II lines. The atmospheres were tailored for each star by interpolating (Masseron 2006) a grid standard of MARCS models (Gustafsson et al. 2008) onto these stellar parameters.

The line selection of titanium can play a large role in some abundance calculations due to uncertain oscillator strengths and blends, as well as difficulties associated with core saturation. Measures were taken to reduce their impact on the overall estimates of titanium abundances, and the final choices are shown in Table A.1. The impact of uncertain oscillator strengths was miti-

gated by using a large selection of lines, assuming the uncertainties to be normally distributed. Spectral lines were fit with one or several Gaussian profiles following Lind et al. (2022), from which their equivalent widths were determined, with blended lines removed essentially via sigma-clipping. Saturated lines were removed by imposing a limit on the reduced equivalent width of $W_{\lambda,\text{red}} = \log_{10}(W_{\lambda}/\lambda) = -4.9$. The final line selection closely resembles that of Scott et al. (2015) for the Sun, Heiter et al. (2015) for Arcturus, and Wood et al. (2013) and Lawler et al. (2013) for the very metal-poor stars. 13-37 Ti I lines and 3-92 Ti II lines were used, depending on the star.

4. Results

4.1. Overview

As anticipated, non-LTE is found to, in general, reduce the strengths of Ti I lines, consistent with over-ionisation. The departure coefficients for the levels lie below 0 (Fig. 5). This translates to positive non-LTE abundance corrections for this species, increasing the titanium abundances inferred from these lines. Compared to Sitnova et al. (2020), Fig. 5 misses several Ti II lines that extend to large departure coefficients. Indeed, this work finds smaller non-LTE effects for Ti II as this would indicate, as it shows a closer coupling to the LTE value of $\log_{10}(\beta) = 0$.

The non-LTE corrections are found to be largest for the very metal-poor giant HD122563, where they can reach over +0.4 dex for certain Ti I lines. For the very metal-poor dwarf and sub-giant, the non-LTE corrections are of the order +0.2 dex. For the Sun, the corrections are more muted, only of the order +0.05 dex. Nevertheless, they have an impact on the ionisation balance (Section 4.2.1). For Arcturus, the abundance corrections are typically of the order +0.01 dex.

For Ti II, the non-LTE corrections are smaller. They can be positive or negative, depending on the transition and on the star. It can be seen that the departure coefficients, given the deeper creation point and majority status of Ti II, exist closer to LTE in almost all cases. The most severe case is HD122563, where certain lines are affected to the +0.2 dex level; this is much lower in all other stars.

In many stars, but most particularly Arcturus, over-saturation was found when analysing the reduced equivalent widths of the lines and their abundance predictions. To counter the inaccurate abundance estimations due to the modified relationship with abundance the saturated lines have, those with a reduced equivalent width of $\log_{10}(W_{\lambda}/\lambda) > -4.9$ were removed, improving the imbalance in all stars but the Sun in LTE. In Arcturus, this left only three Ti II lines, but achieved a better ionisation imbalance nonetheless.

4.2. Abundances and ionisation balance

The mean abundances and ionisation imbalances, $\Delta_{\text{I-II}}$, are presented in Table 2 and Fig. 6. The different stars are discussed individually below.

The differences from Sitnova et al. (2020) are small in LTE, but significant enough to be noted. This could be attributed in part to the difference in the microturbulence parameters in these stars. In this work, they are found to be 0.5 km/s smaller for HD84937, the same for HD140283, and 0.2 km/s larger for HD122563. Indeed, it is found that the discrepancy in LTE abundances with respect to Sitnova et al. (2020) is largest for HD84937 and HD122563. (Table 2).

Table 2. Titanium abundances, $A(\text{Ti})$, and ionisation imbalances, $\Delta_{\text{I-II}}$, found in this work as well as the unweighted values from [Ramírez & Allende Prieto \(2011\)](#) for Arcturus, and from [Sitnova et al. \(2020\)](#) for the other stars.

Star	Species	LTE			Non-LTE		
		Here	Lit.	Diff.	Here	Lit.	Diff.
Sun	Ti I	4.87	4.88	-0.01	4.90	4.91	-0.01
	Ti II	4.92	4.95	-0.03	4.92	4.94	-0.02
	$\Delta_{\text{I-II}}$	-0.06	-0.07	0.02	-0.02	-0.03	0.02
Arcturus	Ti I	4.85	4.66	0.19	4.86	—	—
	Ti II	4.93	4.66	0.27	4.91	—	—
	$\Delta_{\text{I-II}}$	-0.08	0.00	-0.08	-0.05	—	—
HD84937	Ti I	3.20	3.19	0.01	3.40	3.35	0.05
	Ti II	3.20	3.14	0.06	3.21	3.18	0.03
	$\Delta_{\text{I-II}}$	0.00	0.05	-0.05	0.18	0.17	-0.01
HD140283	Ti I	2.69	2.66	0.03	2.91	2.84	0.07
	Ti II	2.69	2.69	0.00	2.71	2.73	-0.02
	$\Delta_{\text{I-II}}$	0.00	-0.03	-0.03	0.20	0.11	0.09
HD122563	Ti I	2.09	2.19	-0.10	2.41	2.40	0.01
	Ti II	2.54	2.58	-0.04	2.57	2.60	-0.03
	$\Delta_{\text{I-II}}$	-0.45	-0.40	-0.05	-0.16	-0.20	0.04

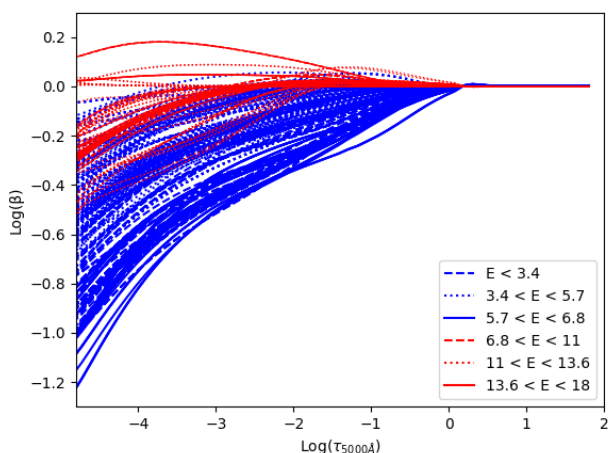


Fig. 5. Departure coefficients of titanium in HD84937 as a function of optical depth. Dotted lines represent Ti II and solid lines represent Ti I. They reach a rough agreement with LTE deeper in the star as collisions dominate. Ti II can be seen to be in closer agreement with LTE than Ti I over all energy levels.

4.2.1. The Sun

In the Sun, the 1D LTE abundances are found to be 4.87 ± 0.01 for Ti I and 4.92 ± 0.01 for Ti II, where the uncertainties reflect the standard error in the mean of the set of diagnostic lines. They are in excellent agreement with the results from [Scott et al. \(2015\)](#), who obtained 4.85 and 4.91, respectively, in LTE using 1D MARCS models. They are also consistent within errors with the 1D LTE results from [Sitnova et al. \(2020\)](#), 4.88 and 4.95 respectively.

With the inclusion of 1D non-LTE effects, the abundances are found to be 4.90 ± 0.01 and 4.92 ± 0.01 for Ti I and Ti II respectively. This is again close to the corresponding abundances in [Sitnova et al. \(2020\)](#), 4.91 and 4.94 respectively.

The 1D LTE abundances correspond to an imbalance of $\Delta_{\text{I-II}} = -0.06 \pm 0.05$ dex. This is small, but significant, especially given that the solar parameters are known precisely. The 1D non-LTE abundances correspond to a much smaller ionisation imbalance, $\Delta_{\text{I-II}} = -0.02 \pm 0.05$ dex. These imbalances are slightly smaller in both magnitude and error than those of [Sitnova et al. \(2020\)](#).

4.2.2. Arcturus

For Arcturus, the non-LTE effects for this mildly metal-poor star are small, as was also found for the Sun (Section 4.2.1). The 1D LTE titanium abundance is found to be 4.82 ± 0.02 from Ti I lines, and 4.93 ± 0.01 from Ti II lines. In non-LTE, they change to 4.83 ± 0.03 for Ti I and 4.90 ± 0.00 for Ti II. These are higher than the [Ramírez & Allende Prieto \(2011\)](#) abundances of 4.66 for both ions, which can in part be explained by the higher microturbulence adopted in that work, and their line selection.

In 1D LTE, Arcturus has a marginally significant titanium ionisation imbalance of $\Delta_{\text{I-II}} = -0.08 \pm 0.08$ dex. In non-LTE, the result is $\Delta_{\text{I-II}} = -0.05 \pm 0.08$ dex.

4.2.3. Very metal-poor giant: HD122563

For HD122563, the 1D LTE titanium abundances are 2.09 ± 0.03 when inferred from Ti I lines, and 2.54 ± 0.02 from Ti II lines. These values are somewhat lower than the 1D LTE values of [Sitnova et al. \(2020\)](#), who find 2.19 for Ti I and 2.58 for Ti II.

The red giant suffers from the largest non-LTE effects: for Ti I they amount to a correction of $+0.32$ dex, such that the titanium abundance increases to 2.41 ± 0.02 . For Ti II the overall correction is just $+0.03$ dex, giving 2.57 ± 0.02 for Ti II. The effects are much larger than those in Arcturus (Section 4.2.2) due to the much lower metallicity of HD122563, which leads to greater over-ionisation.

Although the non-LTE correction on Ti I found here is larger than that found by [Sitnova et al. \(2020\)](#) ($+0.21$ dex), it turns out

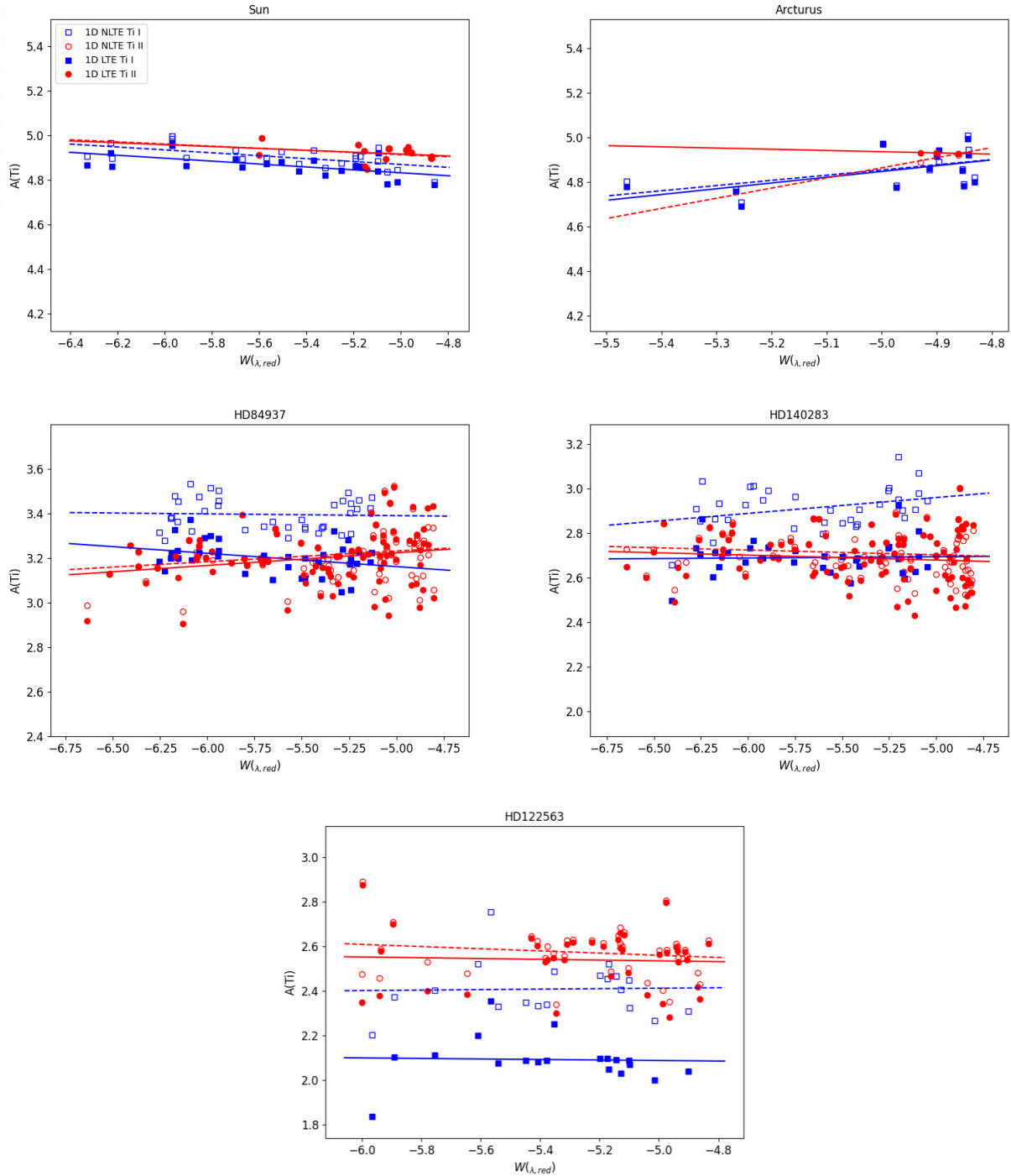


Fig. 6. Difference between the mean abundance of Ti I and Ti II in LTE and non-LTE for all stars, representing the ionisation imbalance. Filled symbols represent LTE and empty symbols non-LTE. Red circles and lines show Ti II and blue squares Ti I. Lines represent the abundance trend, dashed for non-LTE and solid for LTE. The x-axis is the reduced equivalent width: $\log_{10}(W_{\lambda}/\lambda)$.

that the 1D non-LTE abundances from that work and this one are in good agreement; [Sitnova et al. \(2020\)](#) find 2.40 for Ti I and 2.60 for Ti II.

The 1D LTE ionisation imbalance $\Delta_{\text{I-II}}$ is found to also be the most severe of all the stars in this sample: $\Delta_{\text{I-II}} = -0.45 \pm 0.08$ dex. The large non-LTE correction for Ti I, and the correspondingly small correction for Ti II, thus greatly improves this: $\Delta_{\text{I-II}} = -0.16 \pm 0.08$ dex. Hence, it is found that, although 1D non-LTE improves the ionisation imbalance, it does not completely re-

move it. This motivates further study beyond 1D non-LTE for red giants. In other words, 3D non-LTE calculations.

4.2.4. Very metal-poor dwarf and subgiant: HD84937 and HD140283

In 1D LTE, the titanium abundance of HD84937 is measured to be 3.20 ± 0.01 from Ti I lines and 3.20 ± 0.01 from Ti II lines. In 1D non-LTE, the Ti I result increases by $+0.20$ dex to 3.40 ± 0.01 ,

while the Ti II result is almost unchanged at 3.21 ± 0.01 . The correction for Ti I is larger than the $+0.12$ dex found in [Sitnova et al. \(2020\)](#). Nevertheless, the 1D non-LTE abundances found here are consistent with those in that work, at 3.35 and 3.18 from Ti I and Ti II lines, respectively.

The findings for the sub-giant HD140283 are qualitatively similar, with a large 1D non-LTE correction of 0.22 dex for Ti I lines and a smaller one of 0.02 dex for Ti II lines. The 1D non-LTE abundances found here, 2.91 ± 0.01 and 2.71 ± 0.01 respectively, are roughly consistent with those derived by [Sitnova et al. \(2020\)](#), 2.84 and 2.73, respectively.

Titanium ionisation balance is perfectly achieved in 1D LTE for both HD84937 and HD140283: $\Delta_{I-II} = 0.00 \pm 0.05$ dex. Since the Ti I lines suffer a considerable non-LTE effect while the Ti II lines are largely unaffected, this means that a significant ionisation imbalance develops in 1D non-LTE: $\Delta_{I-II} = 0.18 \pm 0.05$ and 0.20 ± 0.05 dex for the two stars, respectively. This was also found in the independent study of [Sitnova et al. \(2020\)](#): 1D non-LTE ionisation imbalances of $\Delta_{I-II} = 0.17$ and 0.11 dex were found for these two stars, whereas the ionisation balance was reduced to 0.05 dex or better in 1D LTE.

5. Conclusion

Titanium abundances in late-type stars have been investigated using 1D model atmospheres and LTE and non-LTE radiative transfer. The present work makes use of an extended model atom that includes new quantum data for inelastic collisions with neutral hydrogen. Promisingly, 1D non-LTE models significantly reduce the ionisation imbalance, Δ_{I-II} , for the Sun (from -0.06 ± 0.05 to -0.02 ± 0.05 dex) and the very metal-poor giant HD122563 (from -0.47 ± 0.08 to -0.17 ± 0.08 dex), relative to 1D LTE. At the same time, however, 1D non-LTE models worsen the ionisation imbalance for the very metal-poor stars HD84937 and HD140283 (by around 0.2 dex). Titanium lines in the mildly metal-poor giant Arcturus were found to form very close to LTE, for which there remains a small ionisation imbalance (-0.08 ± 0.08 dex).

These overall conclusions are broadly consistent with what was previously found by [Sitnova et al. \(2020\)](#), although the non-LTE effects are slightly larger for Ti I and smaller for Ti II. This is reassuring, given that the current work uses a different radiative transfer code, Balder, and a more extended model atom that employs newer data for inelastic Ti I collisions with neutral hydrogen.

It is quite possible that the residual ionisation imbalances for titanium are in part driven by 3D effects, which are significant for the Sun ([Scott et al. 2015](#)). The effect can be expected to be even larger for metal-poor stars, for which the steep temperature gradients should enhance the non-LTE over-ionisation effects ([Amarsi et al. 2016](#); [Nordlander et al. 2017](#)).

Further insight may be gained via a comparison to Fe, for which 1D and 3D non-LTE calculations have been performed. Several studies have found reasonable ionisation balances for HD84937 and HD140283 in 1D non-LTE using either the Drawin formula ([Zhao et al. 2016](#)) or asymptotic models such as those employed in this work ([Amarsi et al. 2016](#)). However, for HD122563, [Amarsi et al. \(2016\)](#) report an ionisation imbalance of around $\Delta_{Fe I-Fe II} = 0.3$ dex in both 1D and 3D non-LTE, similar to the imbalance found in this work for titanium. This may point to as of yet unidentified shortcomings for metal-poor giants, but a larger sample of stars should be analysed before firm conclusions can be drawn. In any case, 3D non-LTE

calculations for titanium will aid in the understanding of these problems.

Acknowledgements. JM and KL acknowledge funds from the European Research Council (ERC) under the European Union's Horizon 2020 research and innovation programme (Grant agreement No. 852977). AMA, JG and PSB acknowledge support from the Swedish Research Council through individual project grants with contract Nos. 2020-03940, 2020-05467 and 2020-03404. This work has made use of the VALD database, operated at Uppsala University, the Institute of Astronomy RAS in Moscow, and the University of Vienna. AKB gratefully acknowledges support from the Russian Science Foundation (the Russian Federation), Project No 22-23-01181.

References

- Amarsi, A. M., Barklem, P. S., Asplund, M., Collet, R., & Zatsarinny, O. 2018a, *A&A*, 616, A89
- Amarsi, A. M., Barklem, P. S., Collet, R., Grevesse, N., & Asplund, M. 2019, *A&A*, 624, A111
- Amarsi, A. M., Lind, K., Asplund, M., Barklem, P. S., & Collet, R. 2016, *MNRAS*, 463, 1518
- Amarsi, A. M., Nordlander, T., Barklem, P. S., et al. 2018b, *A&A*, 615, A139
- Andrievsky, S., Bonifacio, P., Caffau, E., et al. 2018, *MNRAS*, 473, 3377
- Barklem, P., Belyaev, A., Guitou, M., et al. 2011, *Astronomy & Astrophysics - ASTRON ASTROPHYS*, 530
- Barklem, P. S. 2016, *Phys. Rev. A*, 93, 042705
- Barklem, P. S., Belyaev, A. K., & Asplund, M. 2003, *Astronomy and Astrophysics*, 409
- Barklem, P. S., Belyaev, A. K., Dickinson, A. S., & Gad ea, F. X. 2010, *A&A*, 519, A20
- Barklem, P. S., Belyaev, A. K., Spielfiedel, A., Guitou, M., & Feautrier, N. 2012, *A&A*, 541, A80
- Belyaev, A., Vlasov, D., Mitrushchenkov, A., & Feautrier, N. 2019, *Monthly Notices of the Royal Astronomical Society*, 490, 3384
- Belyaev, A. K. 2013, *Phys. Rev. A*, 88, 052704
- Belyaev, A. K. & Barklem, P. S. 2003, *Phys. Rev. A*, 68, 062703
- Belyaev, A. K., Barklem, P. S., Dickinson, A. S., & Gad ea, F. X. 2010, *Phys. Rev. A*, 81, 032706
- Belyaev, A. K., Barklem, P. S., Spielfiedel, A., et al. 2012, *Phys. Rev. A*, 85, 032704
- Belyaev, A. K., Grosser, J., Hahne, J., & Menzel, T. 1999, *Phys. Rev. A*, 60, 2151
- Belyaev, A. K. & Voronov, Y. V. 2018, *ApJ*, 868, 86
- Belyaev, A. K., Yakovleva, S. A., & Kraemer, W. P. 2017, *European Physical Journal D*, 71, 276
- Bensby, T., Feltzing, S., & Oey, M. S. 2014, *A&A*, 562, A71
- Bergemann, M. 2011, *Monthly Notices of The Royal Astronomical Society - MON NOTIC ROY ASTRON SOC*, 413
- Bergemann, M. & Gehren, T. 2008, *Astronomy & Astrophysics*, 492, 823
- Buder, S., Sharma, S., Kos, J., et al. 2021, *MNRAS*, 506, 150
- Cox, A. N. 2000, *Allen's astrophysical quantities* (New York : AIP Press : Springer)
- Dalton, G., Trager, S., Abrams, D. C., et al. 2018, in *Society of Photo-Optical Instrumentation Engineers (SPIE) Conference Series*, Vol. 10702, 107021B
- de Jong, R. S., Agertz, O., Berbel, A. A., et al. 2019, *The Messenger*, 175, 3
- Drawin, H.-W. 1968, *Zeitschrift f ur Physik A Hadrons and nuclei*, 211, 404
- Drawin, H. W. 1969, *Z. Phys.*, 225: 483-93(1969).
- Gaia Collaboration, Prusti, T., de Bruijne, J. H. J., et al. 2016, *A&A*, 595, A1
- Grumer, J. & Barklem, P. S. 2020, *Astronomy & Astrophysics*, 637, A28
- Guitou, M., Spielfiedel, A., Rodionov, D., et al. 2015, *Chemical Physics*, 462, 94
- Gustafsson, B., Edvardsson, B., Eriksson, K., et al. 2008, *A&A*, 486, 951
- Heiter, U., Jofr e, P., Gustafsson, B., et al. 2015, *A&A*, 582, A49
- Helmi, A. 2020, *ARA&A*, 58, 205
- Karovicova, I., White, T. R., Nordlander, T., et al. 2020, *A&A*, 640, A25
- Kaulakys, B. 1991, 24, L127
- Kurucz, R. L. 2016, Robert L. Kurucz on-line database of observed and predicted atomic transitions
- Lambert, D. L. 1993, *Physica Scripta Volume T*, 47, 186
- Lawler, J. E., Guzman, A., Wood, M. P., Sneden, C., & Cowan, J. J. 2013, *ApJS*, 205, 11
- Leenaarts, J. & Carlsson, M. 2009, in *Astronomical Society of the Pacific Conference Series*, Vol. 415, *The Second Hinode Science Meeting: Beyond Discovery-Toward Understanding*, ed. B. Lites, M. Cheung, T. Magara, J. Mariska, & K. Reeves, 87
- Lind, K., Amarsi, A. M., Asplund, M., et al. 2017, *MNRAS*, 468, 4311
- Lind, K., Asplund, M., & Barklem, P. S. 2009, *A&A*, 503, 541
- Lind, K., Nordlander, T., Wehrhahn, A., et al. 2022, *Non-LTE abundance corrections for late-type stars from 2000  to 3 m: I. Na, Mg, and Al*
- Majewski, S. R., Schiavon, R. P., Frinchaboy, P. M., et al. 2017, *AJ*, 154, 94

- Masseron, T. 2006, PhD thesis, Obs. de Paris
- Mihalas, D. 1978, *Stellar atmospheres*
- Nahar, S. 2015, *New Astronomy*, 38
- Nahar, S. 2020, *Atoms*, 8, 68
- Nissen, P. E., Christensen-Dalsgaard, J., Mosumgaard, J. R., et al. 2020, *A&A*, 640, A81
- Nissen, P. E. & Gustafsson, B. 2018, *A&A Rev.*, 26, 6
- Nordlander, T., Amarsi, A. M., Lind, K., et al. 2017, *A&A*, 597, A6
- Olson, R., Smith, F., & Bauer, E. 1971, *Applied Optics*, 10, 1848
- Osorio, Y., Barklem, P. S., Lind, K., et al. 2015, *A&A*, 579, A53
- Przybilla, N., Nieva, M.-F., & Butler, K. 2011, in *Journal of Physics Conference Series*, Vol. 328, *Journal of Physics Conference Series*, 012015
- Prša, A., Harmanec, P., Torres, G., et al. 2016, *The Astronomical Journal*, 152, 41
- Ramírez, I. & Allende Prieto, C. 2011, *The Astrophysical Journal*, 743, 135
- Reggiani, H., Amarsi, Anish M., Lind, Karin, et al. 2019, *A&A*, 627, A177
- Ryabchikova, T., Piskunov, N., Kurucz, R. L., et al. 2015, *Phys. Scr*, 90, 054005
- Scott, P., Asplund, Martin, Grevesse, Nicolas, Bergemann, Maria, & Jacques Sauval, A. 2015, *A&A*, 573, A26
- Shi, J. R., Yan, H. L., Zhou, Z. M., & Zhao, G. 2018, *ApJ*, 862, 71
- Sitnova, T. M., Mashonkina, L. I., & Ryabchikova, T. A. 2016, *Monthly Notices of the Royal Astronomical Society*, 461, 1000
- Sitnova, T. M., Yakovleva, S. A., Belyaev, A. K., & Mashonkina, L. I. 2020, *Astronomy Letters*, 46, 120
- Sitnova, T. M., Yakovleva, S. A., Belyaev, A. K., & Mashonkina, L. I. 2022, *Monthly Notices of the Royal Astronomical Society*, 515, 1510
- Steenbock, W. & Holweger, H. 1984, *Astronomy and Astrophysics*, 130, 319
- van Regemorter, H. 1962, *ApJ*, 136, 906
- Wood, M. P., Lawler, J. E., Sneden, C., & Cowan, J. J. 2013, *The Astrophysical Journal Supplement Series*, 208, 27
- Zhao, G., Mashonkina, L., Yan, H. L., et al. 2016, *ApJ*, 833, 225
- Zhao, G., Zhao, Y.-H., Chu, Y.-Q., Jing, Y.-P., & Deng, L.-C. 2012, *Research in Astronomy and Astrophysics*, 12, 723

Appendix A: Additional table

This section contains the linelists used for both Ti I and Ti II in each star individually, as well as the necessary information on each transition in the model atom.

Table A.1. Lines considered in the analysis, including saturated lines that were removed during final abundance calculation. Errors for equivalent widths were not available for the lines of the Sun from [Scott et al. \(2015\)](#).

Wavelength Å	E_{exc} eV	$\log(gf)$	W_λ mÅ	Error	Abundances	
					LTE	NLTE
Sun						
Ti I						
4281.367	0.813	-1.260	24.000	—	4.84	4.87
4465.805	1.739	-0.130	35.600	—	4.84	4.88
4758.118	2.249	0.510	41.800	—	4.78	4.83
4759.270	2.256	0.590	46.000	—	4.79	4.84
5022.868	0.826	-0.330	69.900	—	4.78	4.78
5113.440	1.443	-0.700	24.500	—	4.82	4.85
5145.460	1.460	-0.540	33.100	—	4.86	4.89
5147.478	0.000	-1.940	34.600	—	4.86	4.90
5152.184	0.021	-1.950	33.200	—	4.86	4.90
5219.702	0.021	-2.220	22.400	—	4.89	4.93
5252.100	0.048	-2.360	16.400	—	4.88	4.92
5295.776	1.067	-1.590	10.600	—	4.89	4.93
5490.148	1.460	-0.840	20.300	—	4.84	4.87
6092.792	1.887	-1.380	3.600	—	4.92	4.96
6258.102	1.443	-0.390	50.500	—	4.92	4.94
6303.757	1.443	-1.580	6.800	—	4.97	5.00
6312.236	1.460	-1.550	6.800	—	4.95	4.98
7357.727	1.443	-1.020	19.900	—	4.87	4.89
8675.372	1.067	-1.500	18.500	—	4.86	4.89
8682.983	1.053	-1.790	10.700	—	4.86	4.89
8692.329	1.046	-2.130	5.200	—	4.86	4.89
8734.710	1.053	-2.240	4.100	—	4.87	4.90
Ti II						
4409.518	1.231	-2.530	38.100	—	4.90	4.89
4444.554	1.116	-2.200	59.900	—	4.90	4.90
4493.522	1.080	-2.780	31.800	—	4.86	4.86
4583.409	1.165	-2.840	30.200	—	4.96	4.96
4609.265	1.180	-3.320	11.600	—	4.91	4.91
4657.201	1.243	-2.290	51.800	—	4.93	4.92
4708.663	1.237	-2.350	50.600	—	4.95	4.95
4719.511	1.243	-3.320	12.200	—	4.99	4.99
4764.525	1.237	-2.690	33.500	—	4.93	4.93
4798.531	1.080	-2.660	42.900	—	4.94	4.94
4865.610	1.116	-2.700	35.000	—	4.85	4.85
5336.786	1.582	-1.600	72.000	—	4.91	4.90
5381.022	1.566	-1.970	56.600	—	4.94	4.93
5418.768	1.582	-2.130	48.100	—	4.94	4.94
84937						
Ti I						
2646.634	0.048	0.060	16.723	0.881	3.22	3.45
2956.132	0.048	0.120	15.147	0.708	3.05	3.30
3186.451	0.000	0.010	18.269	0.249	3.19	3.44
3191.992	0.021	0.160	23.646	0.293	3.22	3.47
3309.496	1.053	-0.190	11.933	0.190	3.14	3.18
3354.633	0.021	0.110	20.764	0.327	3.18	3.42
3370.434	0.000	-0.400	7.455	0.183	3.10	3.36
3371.452	0.048	0.230	24.541	0.311	3.18	3.42
3385.941	0.048	-0.180	10.698	0.197	3.11	3.37

Table A.1. Lines considered in the analysis, including saturated lines that were removed during final abundance calculation. Errors for equivalent widths were not available for the lines of the Sun from [Scott et al. \(2015\)](#).

Wavelength Å	E_{exc} eV	$\log(gf)$	W_λ mÅ	Error	Abundances	
					LTE	NLTE
3635.462	0.000	0.100	20.818	0.243	3.06	3.30
3729.807	0.000	-0.280	12.278	0.169	3.11	3.33
3741.059	0.021	-0.150	15.099	0.198	3.10	3.33
3904.783	0.900	0.150	6.148	0.145	3.13	3.32
3924.526	0.021	-0.870	4.474	0.137	3.21	3.43
3947.768	0.021	-0.890	4.528	0.133	3.23	3.45
3958.205	0.048	-0.110	21.996	0.241	3.28	3.49
3989.758	0.021	-0.130	20.710	0.235	3.24	3.45
3998.636	0.048	0.020	22.842	0.249	3.17	3.40
4008.927	0.021	-1.000	4.184	0.133	3.30	3.51
4024.571	0.048	-0.920	4.603	0.338	3.29	3.50
4025.077	2.153	-1.040	19.407	0.203	3.21	3.21
4287.403	0.836	-0.370	2.993	0.116	3.23	3.36
4305.907	0.848	0.490	20.131	0.231	3.32	3.43
4427.098	1.502	0.230	2.837	0.180	3.20	3.37
4449.142	1.887	0.470	2.994	0.129	3.33	3.47
4518.022	0.826	-0.250	3.747	0.127	3.19	3.32
4533.239	0.848	0.540	17.596	0.200	3.18	3.31
4534.776	0.836	0.350	12.076	0.158	3.16	3.29
4535.569	0.826	0.140	9.021	0.143	3.21	3.34
4548.764	0.826	-0.280	4.395	0.144	3.29	3.41
4555.483	0.848	-0.400	2.536	0.115	3.18	3.31
4617.269	1.749	0.440	2.982	0.111	3.22	3.38
4981.731	0.848	0.570	20.401	0.190	3.21	3.34
4991.066	0.836	0.450	16.413	0.361	3.20	3.32
4999.503	0.826	0.320	13.348	0.168	3.21	3.33
5022.868	0.826	-0.330	2.989	0.115	3.14	3.27
5036.464	1.443	0.140	4.104	0.117	3.37	3.53
5173.743	0.000	-1.060	3.627	0.111	3.20	3.45
5192.969	0.021	-0.950	4.682	0.113	3.23	3.47
Ti II						
2474.194	0.049	-2.420	22.823	1.818	3.44	3.45
2517.431	0.135	-1.500	53.129	4.940	3.58	3.58
2571.032	0.607	-0.900	62.659	7.945	3.74	3.70
2581.711	1.084	-1.580	22.415	1.166	3.49	3.50
2717.297	1.130	-1.490	26.340	5.347	3.52	3.52
2725.773	1.116	-1.550	20.050	1.534	3.40	3.41
2761.287	1.080	-1.350	23.567	0.923	3.27	3.29
2784.638	0.607	-1.990	11.026	0.900	3.03	3.04
2820.361	0.574	-1.910	21.286	0.834	3.29	3.30
2832.176	0.574	-0.850	65.543	2.287	3.65	3.62
2841.935	0.607	-0.590	58.541	3.441	3.19	3.19
2862.319	1.237	-0.530	49.528	4.582	3.35	3.37
2884.102	1.130	-0.230	60.614	1.318	3.35	3.32
3017.183	1.584	-0.300	48.744	0.907	3.36	3.36
3029.728	1.572	-0.350	38.428	0.968	3.08	3.11
3046.684	1.165	-0.810	40.677	1.121	3.23	3.25
3056.738	1.161	-0.790	42.627	1.063	3.27	3.28
3058.088	1.180	-0.420	54.899	1.022	3.32	3.31
3071.239	1.180	-0.750	52.036	0.632	3.49	3.49
3089.400	1.893	0.080	42.717	0.454	3.06	3.12
3103.803	1.892	0.180	51.629	0.712	3.24	3.30
3105.080	1.224	-0.430	52.530	0.787	3.27	3.27
3106.231	1.243	-0.070	56.670	0.543	3.07	3.08
3110.080	1.582	-1.210	12.605	1.576	3.16	3.19
3117.666	1.231	-0.490	41.388	1.879	2.98	3.01
3122.070	1.237	-1.570	11.697	0.540	3.16	3.18

Table A.1. Lines considered in the analysis, including saturated lines that were removed during final abundance calculation. Errors for equivalent widths were not available for the lines of the Sun from [Scott et al. \(2015\)](#).

Wavelength Å	E_{exc} eV	$\log(gf)$	W_λ mÅ	Error	Abundances	
					LTE	NLTE
3144.719	0.113	-2.360	24.452	1.897	3.35	3.35
3154.192	0.113	-1.160	69.833	0.771	3.56	3.49
3184.117	0.012	-2.520	18.383	0.716	3.23	3.23
3197.519	0.028	-1.940	41.150	0.474	3.30	3.28
3203.431	0.000	-1.820	52.780	1.610	3.48	3.44
3213.121	0.012	-2.280	26.246	0.873	3.21	3.21
3214.767	0.049	-1.370	67.276	0.971	3.60	3.51
3224.237	1.584	0.050	53.705	0.554	3.12	3.12
3226.769	0.028	-1.790	52.173	0.718	3.46	3.42
3236.119	1.080	-0.410	53.626	5.112	3.07	3.10
3249.366	1.080	-1.350	27.618	0.442	3.30	3.32
3263.683	1.165	-1.140	26.920	0.394	3.15	3.18
3272.077	1.224	-0.250	51.744	1.237	3.02	3.06
3275.290	1.080	-1.480	16.020	0.224	3.08	3.11
3278.288	1.231	-0.260	58.420	0.502	3.26	3.28
3279.988	1.116	-1.190	28.995	0.699	3.21	3.23
3282.327	1.224	-0.340	52.539	0.561	3.14	3.16
3302.095	0.151	-2.340	20.723	0.304	3.24	3.23
3307.721	0.122	-2.660	12.661	0.204	3.25	3.24
3308.803	0.135	-1.240	68.140	0.518	3.54	3.49
3315.322	1.224	-0.640	44.200	0.578	3.17	3.20
3318.023	0.122	-1.070	73.533	0.530	3.55	3.49
3319.081	0.135	-3.000	7.573	0.178	3.33	3.33
3337.847	1.237	-1.250	19.774	0.279	3.11	3.14
3343.762	0.151	-1.180	69.415	0.495	3.54	3.48
3352.069	1.221	-1.280	22.323	0.298	3.20	3.23
3369.203	1.231	-1.420	15.098	0.212	3.12	3.14
3374.346	1.237	-1.060	28.908	3.204	3.18	3.20
3388.751	1.237	-1.020	27.381	0.364	3.10	3.13
3407.202	0.049	-1.970	39.785	0.969	3.28	3.27
3409.808	0.028	-1.910	43.641	0.506	3.30	3.29
3416.957	1.237	-1.540	11.353	0.230	3.09	3.12
3452.465	2.048	-0.560	15.914	0.262	3.03	3.10
3456.384	2.061	-0.110	30.175	0.368	3.01	3.11
3461.496	0.135	-0.850	82.020	7.164	3.60	3.49
3477.180	0.122	-0.950	80.637	1.814	3.63	3.53
3489.736	0.135	-2.000	42.603	0.469	3.43	3.42
3491.049	0.113	-1.100	74.271	0.491	3.56	3.47
3500.333	0.122	-2.040	32.866	0.354	3.22	3.22
3504.891	1.892	0.380	56.694	1.011	3.12	3.11
3520.252	2.048	-0.180	26.988	0.310	2.98	3.05
3533.854	2.061	-1.310	2.634	0.151	2.91	2.96
3535.407	2.061	0.010	32.222	0.321	2.94	3.02
3561.576	0.574	-2.040	17.707	0.465	3.21	3.21
3573.732	0.574	-1.530	35.625	1.841	3.20	3.19
3596.047	0.607	-1.070	53.092	0.638	3.26	3.21
3741.638	1.582	-0.070	59.641	0.677	3.11	3.14
3757.685	1.566	-0.440	45.258	0.503	3.08	3.12
3759.291	0.607	0.280	118.779	0.718	3.35	3.25
3761.321	0.574	0.180	112.735	0.673	3.32	3.22
3761.872	2.590	-0.420	9.989	0.157	2.97	3.01
3786.323	0.607	-2.600	8.811	0.556	3.31	3.31
3813.388	0.607	-1.890	27.090	0.289	3.22	3.22
3900.539	1.130	-0.290	80.301	0.528	3.49	3.38
3987.606	0.607	-2.730	5.331	0.142	3.18	3.18
4012.384	0.574	-1.780	38.560	0.369	3.32	3.31
4028.338	1.892	-0.920	17.673	0.216	3.14	3.17

Table A.1. Lines considered in the analysis, including saturated lines that were removed during final abundance calculation. Errors for equivalent widths were not available for the lines of the Sun from [Scott et al. \(2015\)](#).

Wavelength Å	E_{exc} eV	$\log(gf)$	W_λ mÅ	Error	Abundances	
					LTE	NLTE
4053.821	1.893	-1.070	13.115	0.171	3.12	3.15
4161.529	1.084	-2.090	8.613	0.148	3.19	3.19
4163.644	2.590	-0.130	23.253	0.242	3.13	3.17
4171.904	2.598	-0.300	18.053	0.208	3.15	3.20
4290.215	1.165	-0.870	53.161	0.593	3.27	3.24
4300.043	1.180	-0.460	72.296	0.782	3.39	3.31
4301.923	1.161	-1.210	38.264	0.418	3.25	3.25
4312.860	1.180	-1.120	42.831	0.503	3.28	3.27
4316.794	2.048	-1.620	3.773	0.122	3.19	3.23
4320.950	1.165	-1.880	13.552	0.406	3.27	3.27
4391.026	1.231	-2.300	6.717	0.141	3.39	3.39
4395.839	1.243	-1.930	9.203	0.146	3.18	3.19
4409.518	1.231	-2.530	2.082	0.116	3.09	3.10
4418.331	1.237	-1.990	8.415	0.142	3.20	3.20
4443.801	1.080	-0.710	69.175	0.448	3.43	3.33
4444.554	1.116	-2.200	6.948	0.131	3.20	3.20
4468.493	1.130	-0.630	71.117	0.462	3.45	3.34
4488.324	3.123	-0.500	4.765	0.133	3.14	3.18
4493.522	1.080	-2.780	1.934	0.111	3.16	3.16
4501.270	1.116	-0.770	65.839	0.474	3.42	3.34
4518.332	1.080	-2.560	4.121	0.132	3.28	3.28
4545.133	1.130	-2.450	3.986	0.133	3.20	3.20
4571.971	1.572	-0.310	63.803	0.423	3.33	3.25
4583.409	1.165	-2.840	1.789	0.103	3.26	3.26
4657.201	1.243	-2.290	4.909	0.147	3.23	3.23
4708.663	1.237	-2.350	4.197	0.114	3.21	3.21
4762.778	1.084	-2.890	1.443	0.119	3.13	3.13
4763.883	1.221	-2.400	4.295	0.120	3.25	3.26
4764.525	1.237	-2.690	2.066	0.106	3.23	3.23
4798.531	1.080	-2.660	2.612	0.198	3.16	3.16
4911.194	3.123	-0.640	3.448	0.110	3.11	3.19
5013.686	1.582	-2.140	4.012	0.136	3.28	3.28
5129.156	1.892	-1.340	9.976	0.154	3.19	3.18
5185.902	1.893	-1.410	8.391	0.136	3.17	3.17
5211.530	2.590	-1.410	1.205	0.097	2.92	2.99
5336.786	1.582	-1.600	10.452	0.138	3.18	3.17
5381.022	1.566	-1.970	5.299	0.141	3.20	3.20
5418.768	1.582	-2.130	3.676	0.153	3.21	3.20
140283						
Ti I						
3981.762	0.000	-0.270	25.044	0.268	2.92	3.14
2646.634	0.048	0.060	21.293	0.479	2.81	3.06
3191.992	0.021	0.160	25.781	0.429	2.69	2.97
3199.914	0.048	0.310	28.752	0.341	2.65	2.94
3309.496	1.053	-0.190	12.151	0.208	2.72	2.77
3354.633	0.021	0.110	22.144	0.310	2.62	2.90
3370.434	0.000	-0.400	9.251	0.198	2.62	2.89
3371.452	0.048	0.230	25.988	0.317	2.62	2.90
3385.941	0.048	-0.180	11.835	0.210	2.57	2.85
3635.462	0.000	0.100	24.615	0.323	2.60	2.86
3729.807	0.000	-0.280	14.543	0.190	2.65	2.90
3741.059	0.021	-0.150	18.645	0.246	2.67	2.92
3904.783	0.900	0.150	6.980	0.147	2.72	2.95
3924.526	0.021	-0.870	4.706	0.152	2.69	2.94
3947.768	0.021	-0.890	5.038	0.150	2.74	2.98
3958.205	0.048	-0.110	22.101	0.221	2.74	3.00

Table A.1. Lines considered in the analysis, including saturated lines that were removed during final abundance calculation. Errors for equivalent widths were not available for the lines of the Sun from [Scott et al. \(2015\)](#).

Wavelength Å	E_{exc} eV	$\log(gf)$	W_λ mÅ	Error	Abundances	
					LTE	NLTE
3989.758	0.021	-0.130	22.249	0.317	2.73	2.98
3998.636	0.048	0.020	25.204	0.273	2.68	2.94
4008.927	0.021	-1.000	4.274	0.133	2.76	3.01
4024.571	0.048	-0.920	3.899	0.172	2.67	2.92
4025.077	2.153	-1.040	18.395	0.199	2.75	2.75
4287.403	0.836	-0.370	1.681	0.107	2.50	2.65
4449.142	1.887	0.470	2.543	0.107	2.86	3.02
4518.022	0.826	-0.250	2.945	0.116	2.60	2.75
4533.239	0.848	0.540	16.912	0.177	2.68	2.82
4534.776	0.836	0.350	11.320	0.158	2.64	2.79
4535.569	0.826	0.140	7.941	0.142	2.67	2.81
4548.764	0.826	-0.280	3.542	0.119	2.71	2.85
4555.483	0.848	-0.400	2.533	0.108	2.70	2.85
4617.269	1.749	0.440	2.450	0.101	2.73	2.90
4981.731	0.848	0.570	18.916	0.195	2.69	2.83
4991.066	0.836	0.450	15.790	0.229	2.69	2.84
4999.503	0.826	0.320	12.664	0.166	2.69	2.84
5022.868	0.826	-0.330	3.346	0.096	2.71	2.86
5173.743	0.000	-1.060	3.636	0.102	2.65	2.93
5192.969	0.021	-0.950	5.308	0.105	2.73	3.00
Ti II						
2474.194	0.049	-2.420	16.588	0.479	2.77	2.78
2571.032	0.607	-0.900	49.930	1.408	2.82	2.82
2725.773	1.116	-1.550	16.545	0.478	2.88	2.89
2761.287	1.080	-1.350	17.913	0.362	2.69	2.71
2784.638	0.607	-1.990	11.018	0.339	2.59	2.60
2832.176	0.574	-0.850	73.872	0.669	3.40	3.38
2841.935	0.607	-0.590	57.579	0.633	2.63	2.66
2862.319	1.237	-0.530	39.353	0.691	2.60	2.65
2884.102	1.130	-0.230	53.627	0.743	2.62	2.64
2888.929	0.574	-1.360	35.823	1.749	2.67	2.70
3029.728	1.572	-0.350	35.125	0.496	2.59	2.63
3046.684	1.165	-0.810	33.755	0.442	2.61	2.65
3056.738	1.161	-0.790	39.140	0.490	2.72	2.75
3058.088	1.180	-0.420	46.472	0.431	2.58	2.62
3089.400	1.893	0.080	36.812	0.592	2.51	2.57
3103.803	1.892	0.180	39.238	0.476	2.46	2.54
3105.080	1.224	-0.430	45.552	0.652	2.59	2.63
3106.231	1.243	-0.070	56.597	0.684	2.59	2.63
3110.080	1.582	-1.210	9.683	0.737	2.64	2.68
3154.192	0.113	-1.160	74.321	0.566	3.12	3.08
3184.117	0.012	-2.520	20.083	0.383	2.78	2.77
3195.715	1.084	-1.390	17.194	0.538	2.62	2.67
3197.519	0.028	-1.940	43.688	1.099	2.83	2.82
3203.431	0.000	-1.820	52.338	1.250	2.93	2.90
3213.121	0.012	-2.280	29.684	0.979	2.78	2.78
3224.237	1.584	0.050	49.048	0.612	2.53	2.57
3226.769	0.028	-1.790	53.110	1.526	2.94	2.91
3263.683	1.165	-1.140	23.765	0.297	2.64	2.69
3272.077	1.224	-0.250	52.508	1.251	2.56	2.62
3275.290	1.080	-1.480	16.374	0.279	2.67	2.71
3276.992	0.122	-2.440	16.969	0.235	2.69	2.69
3278.288	1.231	-0.260	50.905	0.561	2.53	2.59
3279.988	1.116	-1.190	22.024	0.275	2.59	2.63
3282.327	1.224	-0.340	47.776	0.533	2.52	2.57
3302.095	0.151	-2.340	19.755	0.248	2.71	2.71
3307.721	0.122	-2.660	14.970	0.215	2.84	2.84

Table A.1. Lines considered in the analysis, including saturated lines that were removed during final abundance calculation. Errors for equivalent widths were not available for the lines of the Sun from [Scott et al. \(2015\)](#).

Wavelength Å	E_{exc} eV	$\log(gf)$	W_λ mÅ	Error	Abundances	
					LTE	NLTE
3308.803	0.135	-1.240	66.696	0.739	2.91	2.89
3315.322	1.224	-0.640	39.956	0.449	2.60	2.67
3318.023	0.122	-1.070	72.373	0.513	2.91	2.88
3319.081	0.135	-3.000	7.919	0.193	2.86	2.86
3337.847	1.237	-1.250	17.151	0.226	2.61	2.65
3343.762	0.151	-1.180	68.002	0.475	2.89	2.87
3352.069	1.221	-1.280	21.122	0.274	2.75	2.79
3369.203	1.231	-1.420	13.929	0.219	2.66	2.69
3374.346	1.237	-1.060	24.712	3.943	2.64	2.68
3407.202	0.049	-1.970	44.831	0.623	2.86	2.86
3409.808	0.028	-1.910	45.101	0.538	2.79	2.78
3416.957	1.237	-1.540	9.988	0.204	2.61	2.65
3452.465	2.048	-0.560	11.867	0.266	2.52	2.60
3456.384	2.061	-0.110	24.325	0.288	2.49	2.59
3461.496	0.135	-0.850	80.096	5.435	2.90	2.85
3489.736	0.135	-2.000	46.395	0.573	3.00	3.00
3491.049	0.113	-1.100	71.993	0.686	2.86	2.82
3500.333	0.122	-2.040	35.313	0.400	2.75	2.75
3504.891	1.892	0.380	49.854	0.624	2.47	2.52
3520.252	2.048	-0.180	21.796	0.483	2.47	2.55
3533.854	2.061	-1.310	3.172	0.148	2.64	2.69
3535.407	2.061	0.010	27.127	0.313	2.43	2.53
3561.576	0.574	-2.040	15.988	0.270	2.68	2.68
3573.732	0.574	-1.530	35.594	2.193	2.69	2.70
3596.047	0.607	-1.070	52.056	0.556	2.68	2.68
3741.638	1.582	-0.070	53.184	0.610	2.56	2.63
3757.685	1.566	-0.440	37.523	0.387	2.54	2.61
3759.291	0.607	0.280	111.636	0.687	2.75	2.66
3761.321	0.574	0.180	108.670	0.656	2.76	2.67
3761.872	2.590	-0.420	8.304	0.153	2.61	2.65
3786.323	0.607	-2.600	8.394	0.529	2.86	2.87
3813.388	0.607	-1.890	25.384	0.279	2.75	2.75
3900.539	1.130	-0.290	69.866	0.725	2.76	2.70
3913.461	1.116	-0.360	65.483	1.049	2.68	2.64
3981.991	0.574	-2.540	8.381	0.143	2.75	2.75
3987.606	0.607	-2.730	5.223	0.142	2.75	2.75
4012.384	0.574	-1.780	34.284	0.336	2.79	2.79
4028.338	1.892	-0.920	12.998	0.195	2.65	2.70
4053.821	1.893	-1.070	9.145	0.147	2.62	2.67
4161.529	1.084	-2.090	7.348	0.147	2.73	2.74
4163.644	2.590	-0.130	14.121	0.184	2.58	2.65
4171.904	2.598	-0.300	10.990	0.155	2.63	2.69
4290.215	1.165	-0.870	46.801	0.436	2.71	2.72
4300.043	1.180	-0.460	67.900	0.754	2.84	2.81
4301.923	1.161	-1.210	38.424	0.525	2.87	2.87
4316.794	2.048	-1.620	2.012	0.104	2.61	2.67
4320.950	1.165	-1.880	11.160	0.171	2.79	2.80
4330.698	1.180	-2.090	6.467	0.124	2.75	2.76
4418.331	1.237	-1.990	7.433	0.138	2.76	2.78
4443.801	1.080	-0.710	61.977	0.401	2.82	2.76
4444.554	1.116	-2.200	5.172	0.115	2.68	2.68
4450.482	1.084	-1.520	24.059	0.262	2.76	2.75
4468.493	1.130	-0.630	64.215	0.414	2.84	2.78
4488.324	3.123	-0.500	1.828	0.100	2.49	2.53
4493.522	1.080	-2.780	1.295	0.096	2.60	2.61
4501.270	1.116	-0.770	58.311	0.390	2.81	2.77
4518.332	1.080	-2.560	3.297	0.114	2.79	2.80

Table A.1. Lines considered in the analysis, including saturated lines that were removed during final abundance calculation. Errors for equivalent widths were not available for the lines of the Sun from [Scott et al. \(2015\)](#).

Wavelength Å	E_{exc} eV	$\log(gf)$	W_λ mÅ	Error	Abundances	
					LTE	NLTE
4545.133	1.130	-2.450	3.575	0.107	2.77	2.78
4571.971	1.572	-0.310	53.657	0.361	2.69	2.67
4583.409	1.165	-2.840	1.635	0.099	2.84	2.84
4657.201	1.243	-2.290	3.385	0.103	2.69	2.69
4708.663	1.237	-2.350	3.855	0.113	2.80	2.80
4763.883	1.221	-2.400	3.939	0.104	2.84	2.85
4764.525	1.237	-2.690	1.504	0.102	2.71	2.72
4798.531	1.080	-2.660	2.616	0.167	2.77	2.78
5013.686	1.582	-2.140	2.117	0.103	2.64	2.67
5129.156	1.892	-1.340	6.935	0.136	2.69	2.70
5185.902	1.893	-1.410	4.998	0.104	2.60	2.62
5211.530	2.590	-1.410	1.178	0.085	2.65	2.72
5336.786	1.582	-1.600	7.759	0.118	2.68	2.69
5381.022	1.566	-1.970	3.967	0.104	2.72	2.73
5418.768	1.582	-2.130	3.381	0.105	2.82	2.82
Arcturus						
Ti I						
4759.270	2.256	0.590	112.543	1.788	4.77	4.74
4778.255	2.236	-0.350	84.851	1.277	5.02	4.98
4913.613	1.873	0.220	137.628	2.769	5.14	5.09
4915.229	1.887	-0.910	72.443	0.911	4.80	4.74
4926.148	0.818	-2.090	93.792	0.497	4.87	4.83
4997.097	0.000	-2.070	167.350	8.078	5.45	5.48
4999.503	0.826	0.320	238.316	8.286	4.69	4.67
5009.645	0.021	-2.200	159.203	6.120	5.41	5.44
5016.161	0.848	-0.480	174.672	3.573	4.95	4.93
5024.844	0.818	-0.530	176.244	5.328	4.99	4.97
5043.584	0.836	-1.590	123.686	5.131	5.04	5.02
5145.460	1.460	-0.540	135.898	7.219	5.20	5.15
5147.478	0.000	-1.940	181.900	11.725	5.63	5.65
5230.967	2.239	-1.190	29.035	0.177	4.69	4.66
5282.376	1.053	-1.810	101.973	0.890	5.04	5.02
5300.010	1.053	-2.300	75.916	0.836	4.99	4.98
5338.306	0.826	-2.730	67.137	1.479	4.91	4.88
5366.639	0.818	-2.460	75.554	2.440	4.78	4.74
5384.630	0.826	-2.770	57.245	0.779	4.78	4.75
5453.642	1.443	-1.600	76.460	2.076	4.85	4.80
5465.773	1.067	-2.910	29.690	0.205	4.76	4.75
5471.192	1.443	-1.420	88.090	0.473	4.89	4.82
5866.451	1.067	-0.790	162.541	2.731	5.08	5.06
5918.536	1.067	-1.640	111.474	0.589	4.94	4.92
5922.110	1.046	-1.380	127.487	1.442	4.93	4.94
5937.809	1.067	-1.940	95.440	0.507	4.91	4.92
6091.171	2.267	-0.320	87.629	0.475	4.92	4.84
6336.099	1.443	-1.690	77.201	0.419	4.86	4.79
6395.472	1.502	-2.540	22.009	0.152	4.78	4.76
6497.684	1.443	-2.020	65.279	0.363	4.97	4.92
6554.223	1.443	-1.150	117.196	0.666	4.99	4.89
6556.062	1.460	-1.060	128.324	1.458	5.11	5.02
8692.329	1.046	-2.130	110.286	2.062	4.94	4.86
Ti II						
4798.531	1.080	-2.660	106.218	12.979	5.06	5.06
4865.610	1.116	-2.700	107.891	2.043	5.18	5.18
4874.009	3.095	-0.860	57.401	0.589	4.93	4.79
5005.167	1.566	-2.730	68.903	2.361	4.93	4.92
5211.530	2.590	-1.410	65.531	1.450	4.93	4.92

Table A.1. Lines considered in the analysis, including saturated lines that were removed during final abundance calculation. Errors for equivalent widths were not available for the lines of the Sun from [Scott et al. \(2015\)](#).

Wavelength Å	E_{exc} eV	$\log(gf)$	W_λ mÅ	Error	Abundances	
					LTE	NLTE
122563						
Ti I						
3598.714	0.900	-0.610	9.777	0.220	2.35	2.74
3725.152	1.067	-0.340	4.023	0.142	1.84	2.19
3729.807	0.000	-0.280	62.128	0.445	2.06	2.42
3741.059	0.021	-0.150	60.851	0.428	1.91	2.30
3752.858	0.048	0.050	74.038	0.929	2.03	2.40
3904.783	0.900	0.150	26.459	0.363	2.05	2.51
3924.526	0.021	-0.870	29.245	0.373	2.03	2.40
3947.768	0.021	-0.890	31.212	0.770	2.09	2.44
3958.205	0.048	-0.110	73.019	2.408	2.10	2.48
3998.636	0.048	0.020	75.584	1.503	2.01	2.40
4008.927	0.021	-1.000	26.877	0.330	2.10	2.44
4025.077	2.153	-1.040	90.895	0.846	2.77	2.78
4287.403	0.836	-0.370	19.025	0.231	2.25	2.48
4449.142	1.887	0.470	5.708	0.152	2.10	2.35
4518.022	0.826	-0.250	18.905	0.202	2.09	2.33
4534.776	0.836	0.350	43.721	0.333	2.00	2.25
4535.569	0.826	0.140	36.210	0.479	2.07	2.31
4548.764	0.826	-0.280	17.749	0.190	2.08	2.32
4555.483	0.848	-0.400	13.090	0.158	2.08	2.32
4617.269	1.749	0.440	8.111	0.138	2.11	2.37
4981.731	0.848	0.570	62.468	0.396	2.04	2.30
5022.868	0.826	-0.330	17.917	0.195	2.09	2.34
5036.464	1.443	0.140	12.377	0.162	2.20	2.51
5173.743	0.000	-1.060	32.679	0.316	2.10	2.46
5192.969	0.021	-0.950	37.243	0.333	2.09	2.46
Ti II						
3500.333	0.122	-2.040	99.922	2.727	2.68	2.70
3533.854	2.061	-1.310	15.915	0.250	2.30	2.34
3535.407	2.061	0.010	66.974	1.476	2.10	2.19
3757.685	1.566	-0.440	83.136	2.103	2.20	2.33
3759.291	0.607	0.280	209.168	1.279	2.62	2.62
3761.321	0.574	0.180	194.250	4.133	2.56	2.57
3761.872	2.590	-0.420	34.370	0.552	2.38	2.44
3774.647	0.574	-2.650	55.363	3.764	2.61	2.63
3776.053	1.582	-1.240	51.734	0.689	2.36	2.43
3813.388	0.607	-1.890	100.697	5.068	2.88	2.91
3900.539	1.130	-0.290	133.115	0.853	2.74	2.72
3987.606	0.607	-2.730	48.878	0.636	2.58	2.58
4012.384	0.574	-1.780	103.308	2.660	2.73	2.74
4028.338	1.892	-0.920	54.402	0.386	2.42	2.48
4053.821	1.893	-1.070	41.757	0.460	2.34	2.40
4161.529	1.084	-2.090	51.710	0.594	2.54	2.56
4163.644	2.590	-0.130	45.062	0.480	2.28	2.35
4316.794	2.048	-1.620	18.131	0.207	2.54	2.60
4330.698	1.180	-2.090	49.565	0.624	2.60	2.61
4391.026	1.231	-2.300	46.454	0.470	2.80	2.80
4395.839	1.243	-1.930	51.120	0.621	2.53	2.55
4409.518	1.231	-2.530	21.144	0.293	2.54	2.56
4418.331	1.237	-1.990	51.096	0.348	2.58	2.60
4444.554	1.116	-2.200	47.123	0.503	2.57	2.58
4488.324	3.123	-0.500	10.120	0.159	2.38	2.41
4493.522	1.080	-2.780	18.654	0.202	2.53	2.55
4518.332	1.080	-2.560	32.997	0.353	2.63	2.65
4545.133	1.130	-2.450	33.627	0.282	2.59	2.61

Table A.1. Lines considered in the analysis, including saturated lines that were removed during final abundance calculation. Errors for equivalent widths were not available for the lines of the Sun from [Scott et al. \(2015\)](#).

Wavelength Å	E_{exc} eV	$\log(gf)$	W_λ mÅ	Error	Abundances	
					LTE	NLTE
4583.409	1.165	-2.840	16.976	0.221	2.64	2.65
4609.265	1.180	-3.320	5.332	0.116	2.58	2.59
4657.201	1.243	-2.290	34.988	0.629	2.59	2.60
4708.663	1.237	-2.350	36.021	0.280	2.65	2.66
4719.511	1.243	-3.320	6.008	0.130	2.70	2.71
4763.883	1.221	-2.400	35.184	0.346	2.66	2.68
4764.525	1.237	-2.690	18.544	0.198	2.60	2.62
4798.531	1.080	-2.660	28.559	0.650	2.62	2.63
4865.610	1.116	-2.700	24.999	0.249	2.62	2.63
4874.009	3.095	-0.860	4.867	0.123	2.35	2.40
4911.194	3.123	-0.640	8.161	0.129	2.40	2.45
5013.686	1.582	-2.140	22.092	0.212	2.55	2.57
5129.156	1.892	-1.340	40.354	0.823	2.48	2.50
5185.902	1.893	-1.410	35.635	0.319	2.47	2.49
5211.530	2.590	-1.410	5.966	0.111	2.38	2.46
5336.786	1.582	-1.600	53.625	0.370	2.56	2.58
5381.022	1.566	-1.970	34.910	0.280	2.60	2.61
5396.247	1.584	-3.180	5.427	0.112	2.88	2.89
5418.768	1.582	-2.130	26.487	0.208	2.61	2.62